Quadruple junction polymer solar cells with four complementary absorber layers

ADVANCED MATERIALS

www.advmat.de

Quadruple Junction Polymer Solar Cells with Four Complementary Absorber Layers

*Dario Di Carlo Rasi, Koen H. Hendriks, Martijn M. Wienk, and René A. J. Janssen**

A monolithic two-terminal solution-processed quadruple junction polymer solar cell in an n–i–p (inverted) configuration with four complementary polymer:fullerene active bulk-heterojunction layers is presented. The subcells possess different optical bandgaps ranging from 1.90 to 1.13 eV. Optical modeling using the transfer matrix formalism enables prediction of the fraction of absorbed photons from sunlight in each subcell and determine the optimal combination of layer thicknesses. The quadruple junction cell features an open-circuit voltage of 2.45 V and has a power conversion efficiency of 7.6%, only slightly less than the modeled value of 8.2%. The external quantum efficiency spectrum, determined with appropriate light and voltage bias conditions, exhibits in general an excellent agreement with modeled spectrum. The device performance is presently limited by bimolecular recombination, which prevents using thick photoactive layers that could absorb light more efficiently.

Thin film organic solar cells are an emerging technology for flexible, bendable, and stretchable photovoltaic applications,[1–3] for which traditional crystalline silicon technology cannot be applied. In addition, organic semiconductors allow for color tuning and for making devices that are semi-transparent in the visible range.[4–6] The most efficient concept for organic solar cells is the so-called bulk-heterojunction, which comprises an interpenetrating network of electron-donating and electron-accepting semiconductors, intimately mixed at a domain size of few tens of nanometers.[7] Organic solar cells can either be processed by thermal evaporation of small molecules in high vacuum or via solution processing of small molecules or polymers. The latter allows the fabrication of large-area devices using low-cost printing techniques such as slot-dye and spray coating.[8,9] The power conversion efficiency (PCE) of solution-processed organic solar cells has increased significantly in the last decade, reaching the 14% threshold recently.[10,11]

Single absorber layers have a well-defined bandgap and this has two important consequences on the achievable efficiency. First, photons with energy lower than the bandgap are transmitted through the active material and do not contribute to the production of current. Second, photons with energy higher than the bandgap are not efficiently exploited since the resulting excess energy is lost by thermalization to the bandgap energy. An elegant solution to overcome these limitations is provided by multijunction solar cells, which combine complementary bandgap absorbers in adjacent subcells. High energy photons are first absorbed by a wide bandgap absorber, and those with lower energy are transmitted and absorbed by the next absorber in the series which has a smaller bandgap. The efficiency of multijunction solar cells can be progressively increased by stacking an increasing number of absorbers.[12] Following this approach, crystalline semiconductor quintuple junction solar cells and quadruple junction thin film solar cells using amorphous silicon have reached PCEs of 38.8% and 15.0%, respectively.[13,14]

Several solution-processed monolithic tandem and triple junction organic solar cells have been reported.[15,16] A record PCE of 15% was recently reported for a 2 mm^2 organic tandem cell with a visible absorbing front subcell grown by vacuum thermal evaporation and a solution-processed infrared absorbing back subcell.[17] In multijunction solar cells, two or more organic photoactive layers are connected in series by means of an interconnection layer (ICL) where electrons and holes of two adjacent subcells recombine to sustain the photocurrent through the entire stack. This interconnection or recombination layer, which can be partially or entirely processed from solution, connects the two subcells electrically and optically. Solution-processed multijunction organic solar cells with more than three active layers have been reported in very few occasions, and in such cases the same absorber layer was repeated along the stack.[18,19] Given the lack of complementarity in the absorption spectra of the subcells, these multijunction cells did not offer the opportunity to achieve a high efficiency.

Here, we report a first example of a quadruple junction polymer solar cell that features four complementary bandgap absorber

D. Di Carlo Rasi, Dr. K. H. Hendriks, Dr. M. M. Wienk, Prof. R. A. J. Janssen
Molecular Materials and Nanosystems
Institute for Complex Molecular Systems
Eindhoven University of Technology
P.O. Box 513, 5600 MB Eindhoven, The Netherlands
E-mail: r.a.j.janssen@tue.nl

Dr. K. H. Hendriks, Dr. M. M. Wienk, Prof. R. A. J. Janssen
Dutch Institute for Fundamental Energy Research
De Zaale 20, 5612 AJ Eindhoven, The Netherlands

The ORCID identification number(s) for the author(s) of this article can be found under https://doi.org/10.1002/adma.201803836.

DOI: 10.1002/adma.201803836

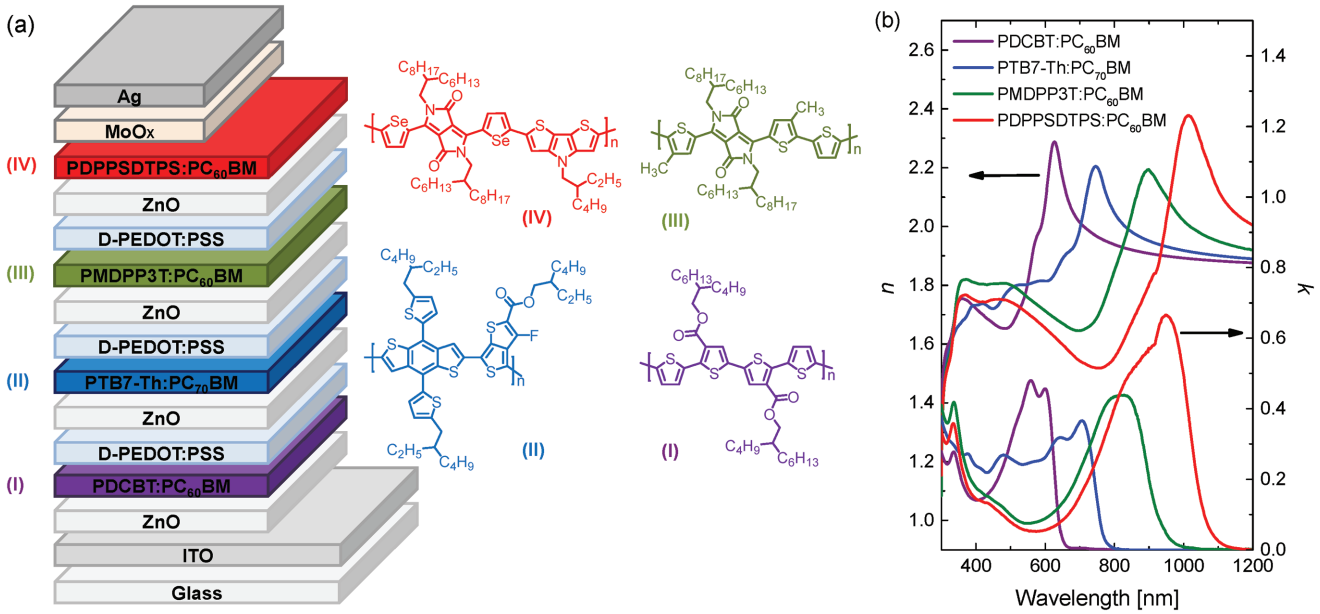

Figure 1. a) Device structure of the quadruple junction solar cell and chemical structure of the photoactive polymers featured in each subcell: (I) PDCBT:$PC_{60}BM$, (II) PTB7-Th:$PC_{70}BM$, (III) PMDPP3T:$PC_{60}BM$, and (IV) PDPPSDTPS:$PC_{60}BM$. b) Wavelength-dependent *n* and *k* optical constants of the active layers used for the quadruple junction.

layers (**Figure 1**a). The device comprises 14 functional layers of which 11 are processed consecutively from solution. The subcells were fabricated using four different polymer:fullerene active layers with optical bandgaps (E_g) ranging from 1.90 to 1.13 eV and a combination of poly(3,4-ethylenedioxythiophene):polystyrene sulfonate (PEDOT:PSS) and ZnO as interconnection layer in an n–i–p (inverted) configuration (Figure 1a). The quadruple junction solar cells reached a PCE of 7.6% with an open-circuit voltage of 2.45 V. The external quantum efficiency (EQE) of the quadruple junction solar cells was measured using bias light of different wavelengths, following a protocol that involves optical modeling and correcting for the build-up electric field.[20]

The first cell on top of the transparent indium tin oxide (ITO)/ZnO contact consists of poly[5,5′-bis(2-butyloctyl)-(2,2′-bithiophene)-4,4′-dicarboxylate-alt-5,5′-2,2′-bithiophene] (PDCBT) with E_g = 1.90 eV as donor,[21] blended with [6,6]-phenyl-C_{61}-butyric acid methyl ester ($PC_{60}BM$) as acceptor. The second photoactive layer is poly[4,8-bis(5-(2-ethylhexyl)thiophen-2-yl)benzo[1,2-*b*:4,5-*b*′]dithiophene-co-3-fluorothieno[3,4-*b*]-thiophene-2-carboxylate] (PTB7-Th) having E_g = 1.58 eV in combination with [6,6]-phenyl-C_{71}-butyric acid methyl ester ($PC_{70}BM$).[22] The third subcell comprises poly[[2,5-bis(2-hexyldecyl-2,3,5,6-tetrahydro-3,6-dioxopyrrolo[3,4-*c*]pyrrole-1,4-diyl]-*alt*-[3′,3″-dimethyl-2,2′:5′,2″-terthiophene]-5,5″-diyl] (PMDPP3T) with E_g = 1.30 eV together with $PC_{60}BM$.[23] Finally, the device is completed with a subcell consisting of poly[[4-(2-ethylhexyl)-4*H*-dithieno[3,2-*b*:2′,3′-*d*]pyrrole-2,6-diyl]-*alt*-2,5-selenophenediyl[2,5-bis(2-ethylhexyl)-2,3,5,6-tetrahydro-3,6-dioxopyrrolo[3,4-*c*]-pyrrole-1,4-diyl]-2,5-selenophenediyl] (PDPPSDTPS), having a small bandgap of E_g = 1.13 eV, combined with $PC_{60}BM$ as acceptor.[24] To interconnect these cells, we use layers of PEDOT:PSS, deposited from the commercial dispersion, diluted with *n*-propanol to near azeotropic composition (referred to as D-PEDOT:PSS) as hole transport layer, and ZnO nanoparticles, dispersed in isoamyl alcohol, as electron transport layer.[25] Details about the processing are in the Experimental Section.

The efficiency of the quadruple junction solar cell strongly depends on the appropriate matching of the current generation in each of the individual subcells. To determine the optimal layer thicknesses for the quadruple junction solar cell, we used a combination of experiments on representative single junction cells (Figure S1, Supporting Information) together with optical modeling using the transfer matrix (TM) formalism. To this end, we determined the wavelength-dependent refractive index $n(\lambda)$ and extinction coefficient $k(\lambda)$ for each photoactive layer (Figure 1b), the charge-transport layers (D-PEDOT:PSS, MoO_x, and ZnO), and the electrodes (ITO, Ag). Second, the photovoltaic performance of the four individual photoactive layers was determined as a function of the layer thickness using single junction cells. The details of these experiments can be found in Tables S1–S4 in the Supporting Information. By using optical simulations for the single junction cells, it is possible to model the fraction of photons absorbed by the photoactive layers ($f_A(\lambda)$), and by combining this with the experimental EQE(λ), we determined the internal quantum efficiency (IQE(λ)) for each layer. With these data, it is possible to predict the performance of the quadruple solar cell for each thickness combination under AM1.5G illumination. In the optical simulations, we used a 45 nm thick D-PEDOT:PSS layer and a 15 nm layer of ZnO nanoparticles, which correspond to the experimentally used thicknesses. The simulations reveal that for a layer thickness combination of 110, 100, 170, and 160 nm for the front, front-middle, back-middle, and back cells, respectively, a PCE of 8.2% can be expected (**Table 1**). **Figure 2** shows the corresponding fraction of photons absorbed by the photoactive layers, the parasitic absorption by the charge-transport layers

Table 1. Modeled and experimental device metrics of the quadruple junction solar cell under AM1.5G (100 mW cm^{-2}) illumination.

	J_{SC} [mA cm^{-2}]	V_{OC} [V]	FF	PCE [%]
Modeling	5.26	2.46	0.63	8.2
Experiment	5.23	2.45	0.59	7.6

and the electrodes, and the fraction of unused (i.e., reflected) photons. The spectrum of the fraction of absorbed photons is a combination of absorption and interference effects. Figure 2 shows that the parasitic absorption is largely situated in near-IR region and dominated by the three D-PEDOT:PSS layers and the ITO electrode. The appreciable absorption of light in the UV region by ITO and ZnO is less relevant for the device performance because the sun's photon flux is small in the UV region. **Table 2** shows the expected current generation in each of the four subcells under AM1.5G (100 mW cm^{-2}) illumination. These currents were determined from the modeled EQE spectra (**Figure 3**b) that were calculated by multiplying the modeled fraction of absorbed photons, $f_A(\lambda)$, in each photoactive layer with the IQE(λ) of that layer. Subsequent integration with the AM1.5G spectrum over all wavelengths afforded the expected short-circuit current densities (J_{SC}) values. Table 2 reveals that the J_{SC}s of the subcells are similar, but not perfectly matched, and that the back cell is current limiting.

To ensure sufficient accuracy in measuring the J–V characteristic, we matched the light source of our solar simulator in such a way that, at the thicknesses used in the quadruple junction device, the corresponding four single junction cells generated virtually the same J_{SC} under solar simulator as the value obtained by integration of their EQE spectrum with the AM1.5G solar spectrum. The photovoltaic performance characteristics of the representative cells, fabricated in the same run of the quadruples, are collected in Table S5 and Figure S2 in the Supporting Information.

The measurement of the quadruple junction devices under the calibrated light source returned in the best case a V_{OC} of 2.45 V, a J_{SC} of 5.23 mA cm^{-2}, and a fill factor (FF) of 0.59 (Figure 3a, Table 1). Together, these corresponded to a PCE of 7.6%, which matches the expected efficiency of 8.2% rather well. There is an excellent match between the modeled and experimental values for J_{SC} and V_{OC} and only the FF is slightly less than expected (0.59 vs 0.63, see Table 1). Hence, the interconnecting contact of D-PEDOT:PSS/ZnO does not lead to voltage losses. The slightly lower FF can be due to small resistive losses in the interconnecting layers, which are not accounted for in the modeling. Due to the intricate device fabrication, involving 11 solution-processed layers, the yield of efficient quadruple solar cells is moderate: 6 out of 16 devices had efficiencies above 7% with an average of 7.3 ± 0.2%. Figure S3 in the Supporting Information shows the distribution of PCEs among all 16 devices.

To obtain more insight on the device operation, we measured the EQEs of each subcell. Measuring the EQE of a specific subcell in a two-terminal quadruple junction solar cell requires that this subcell is current limiting over the entire wavelength range over which it is measured. This can be accomplished by using appropriate bias illumination for the remaining three subcells. Optically biased subcells, however, induce an electric field in the device, which brings the current-limiting subcell in the reverse bias regime.[26] Because the photocurrent in polymer solar cells depends on the applied voltage, this can result in an overestimation of the short-circuit current density and EQE. To correct this, a suitable bias voltage should be applied to the quadruple junction solar cell to compensate for this optically induced electric field over the subcell of interest. To determine the correct bias illumination conditions, we used optoelectrical modeling,[20] and the results are collected in Table S6 in the Supporting Information. We approximated the bias voltage corrections as the sum of the V_{OC}s of the representative single junction cells measured under AM1.5G illumination (see the Experimental Section). In practice, this differs by only few tens of mV from the actual values.[20] Figure 3b shows the EQE measurements of the quadruple device measured under representative light and voltage bias conditions (open markers). Figure S4 in the Supporting Information shows three additional EQE spectra for nominally identical quadruple-junction cells fabricated on different substrates. Thanks to the judiciously selected light bias conditions, it possible to measure the EQE of each individual subcell. Figure S4 in the Supporting Information demonstrates that the voltage correction during the

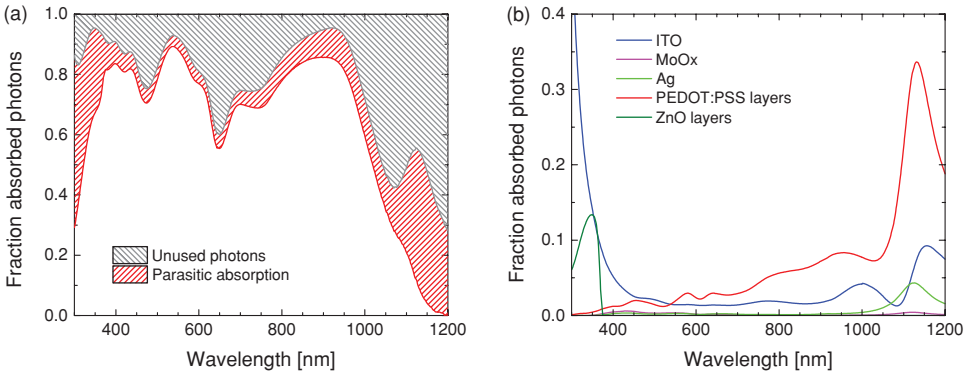

Figure 2. a) Fraction of photons absorbed by the active layers (white background), parasitic absorption by non-photoactive layers (red hatched area), and fraction of unused (i.e., reflected) photons (black hatched area) as determined by optical modeling calculations using the TM method. b) Individual contributions of the different non-photoactive layers to the parasitic absorption.

Table 2. EQE-integrated J_{SC} [mA cm^{-2}] of the subcells of the quadruple junction device.

	Front cell	Middle-front cell	Middle-back cell	Back cell
Modeling	6.45	5.25	6.68	4.57
Experiment	6.21	4.77	5.17	4.55

EQE measurement is important to not overestimate the EQEs. The measurement without any light bias effectively follows the lower envelope of the EQEs and suggests that leakage paths are not significant (Figure S4, Supporting Information).[27]

To give credence to these measurements, the EQE spectra in Figure 3b are compared to the curves expected from the fraction of absorbed photons from the AM1.5G spectrum multiplied by the wavelength-dependent IQE of each photoactive layer. With the exception of the PMDPP3T:$PC_{60}BM$ middle-back cell, the agreement between experiment and modeling is outstanding.

For the deviating middle-back cell, we investigated whether the internal quantum efficiency of that active layer was affected by the processing of the back cell. To this end, we fabricated different single junction devices with the structure: ITO/ZnO/PMDPP3T:$PC_{60}BM$/Top contact. For the top contact, we compared different stacks like MoO_X/Ag (1), D-PEDOT:PSS/MoO_X/Ag (2), and D-PEDOT:PSS/ZnO/Ag (3). For device (2), a second version (2′) was made in which the D-PEDOT:PSS layer was rinsed first with butanol and then with a mixture of chloroform with 5 vol% *o*-dichlorobenzene, from which the top back-cell of PDPPSDTPS:$PC_{60}BM$ in the quadruple was processed. For device (3′), the top ZnO layer was rinsed only with the same chloroform/*o*-dichlorobenzene mixture as for (2′). Figure S5 in the Supporting Information shows the *J*–*V* characteristic of these cells under simulated AM1.5G light. No difference can be noticed between the pristine devices and the rinsed ones. A minor loss in J_{SC} from configuration (1) to (2) to (3) appears, due to D-PEDOT:PSS and ZnO, which act as optical spacers. Given these results, we cannot confirm that the processing conditions used for the back cell deteriorate the performance of the middle-back cell.

With a PCE of 7.6%, the quadruple junction cell has an efficiency that is lower than that of the best single, tandem, and triple junction cells reported to date. Several factors contribute to this. Apart from reflection losses and parasitic absorption, the EQE data in Figure 3b clearly show that the middle-front, middle-back, and back cell all use photons that should have been absorbed by the previous layer in the stack. At the layer thicknesses used (100–170 nm), the photoactive materials are unable to have unit absorption. Single junction cells are more forgiving in this sense because photons that are not absorbed in their first pass will be reflected by the metal back electrode, and can be absorbed in the second pass. For multijunction cells, these photons are more likely to be absorbed by a subsequent layer. At present, the only way to increase the absorption efficiency of individual layers is to increase the thickness. Unfortunately, the performance of organic bulk-heterojunction cells is affected by bimolecular recombination, which increases with layer thickness and lowers the fill factor (**Figure 4**), and in turn, the efficiency. Hence, while multijunction polymer solar cells offer the perspective of reaching PCEs in excess of 20%, accomplishing such goal hinges on developing photoactive layers which absorb more efficiently and provide less bimolecular recombination.

In conclusion, we combined four different photoactive polymers with complementary absorption spectra to fabricate a first example of a quadruple junction polymer solar cell via solution processing. The quadruple junction solar cell provided a PCE of 7.6% under simulated AM1.5G sunlight. The results were validated by comparison with modeling, using the *J*–*V* characteristics of representative single junction cells and optical modeling to determine the fraction of absorbed photons in each individual layer. The correspondence between the measured and modeled EQE was excellent in terms of predicting the spectral shapes and height, except for the middle-back cell where the experimental EQE was lower. The efficiency of the quadruple junction polymer cell is limited by bimolecular recombination in the photoactive layers, which prevents the use of thick (>200 nm) layers to absorb light more efficiently. Improving the efficiency of multijunction cells, therefore, hinges on developing materials that are efficient also for thick layers. From the perspective of the device fabrication, the present work demonstrates that it possible to process complex device stacks (in this case, 14 individual layers of which 11 are processed

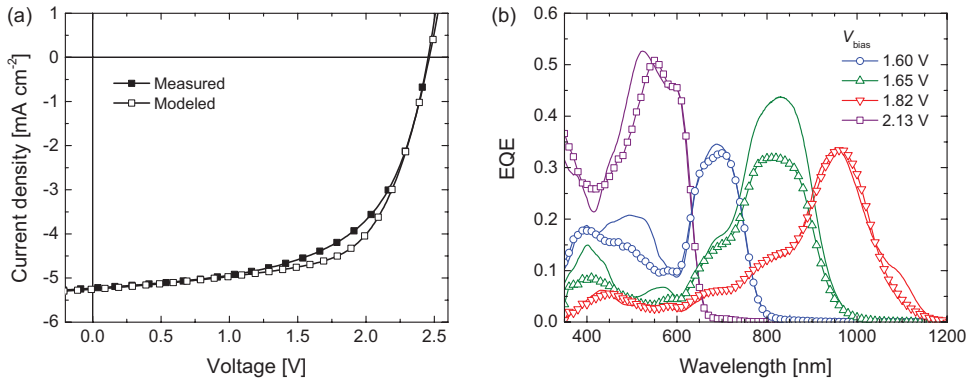

Figure 3. Modeled and experimental device characteristics of the quadruple junction solar cell. a) *J*–*V* characteristics under simulated AM1.5G (100 mW cm^{-2}) illumination. b) Modeled (solid lines) and experimental (lines with open markers) EQEs. The experimental EQEs were measured under representative light and voltage bias conditions.

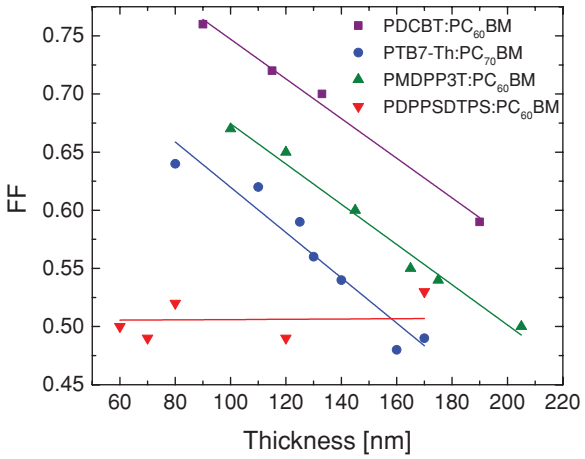

Figure 4. FF of representative single junction cells as a function of the thickness of the active layer. Lines are guides to the eye.

from solution) in a reliable fashion with photovoltaic properties that are in very good agreement with the expected values. This provides the framework for the development of efficient complex multijunction solar cells from solution.

Experimental Section

Materials: Pre-patterned ITO (170 nm) on glass substrates were purchased from Naranjo Substrates. Molybdenum trioxide (MoO_3) powder (99.97%) was purchased from Sigma Aldrich. The ZnO layers were made via a sol–gel route or by spin coating a suspension of preformed nanoparticles in isoamyl alcohol.[25] The former consisted of a solution of 0.5 M $Zn(CH_3COO)_2{\cdot}2H_2O$ (98%, Acros Organics) and 0.5 M ethanolamine in 2-methoxyethanol. The suspension of PEDOT:PSS (Clevios P, VP AI 4083) was diluted in 1-propanol 1:2 v/v right before use, referred to in the main text as D-PEDOT:PSS.[25] PDCBT,[21] PMDPP3T,[23] and PDPPSDTPS[24] were synthesized according to procedures reported in literature. PTB7-Th was purchased from 1-Material (batch YY10228).

Device Fabrication: The patterned ITO substrates were cleaned by sonication in acetone, followed by a solution of sodium dodecyl sulfate in water. They were then rinsed in water and sonicated in isopropanol before being treated under a UV/ozone lamp to complete the cleaning. In the following paragraphs, the processing of all the layers made from solution is described. Wherever mentioned, the sol–gel ZnO was cast directly on clean ITO substrates by spin coating in ambient air and annealed at 150 °C for 5 min on a hotplate. The D-PEDOT:PSS solution was always processed by dynamic spin coating (90 µL per sample) in a N_2–filled glove box for improved wetting to form a 45 nm thick layer. The layer was kept in the vacuum of the antechamber for 30 min right after spin coating to remove residual solvents and no further treatment was performed. The ZnO nanoparticle dispersion was dynamically spin coated (70 µL per sample) in ambient air to give a 15 nm thick layer, without any post-treatment. The last step in the fabrication of each of these devices was the evaporation of the top contact. In all cases, this was accomplished by evaporating MoO_X (10 nm), followed by Ag (100 nm) in a vacuum chamber at $\approx 6 \times 10^{-7}$ mbar, through a shadow mask. On each substrate, the intersection of the ITO pattern with the evaporated top contact formed two squares of 9 mm^2 area and two squares of 16 mm^2 area. The thickness of each layer was measured using a Veeco Dektak profilometer.

PDCBT:PC_{60}BM Single Junction Cells: The clean ITO substrates were covered with ZnO from the sol–gel route. The two components blended in a 1:1 weight ratio were dissolved in chloroform containing 1 vol% of *o*-dichlorobenzene at a concentration of 10 mg mL^{-1} of polymer. Subsequently, the solution of PDCBT:PC_{60}BM was spin coated in a N_2-filled glove box to form a layer with a thickness of 110 nm. The substrates were then annealed in the glove box for 10 min at 100 °C. After this step, the D-PEDOT:PSS solution was spin coated and the samples annealed again at 105 °C for 10 min.

PTB7-Th:PC_{70}BM Single Junction Cells: D-PEDOT:PSS was processed directly on clean ITO substrates and annealed at 105 °C for 10 min in the glove box. Then the ZnO nanoparticles were deposited as previously described; PTB7-Th was mixed with $PC_{70}BM$ (1:1.5 weight ratio) and dissolved in chlorobenzene, containing 3 vol% diiodooctane at a concentration of 12 mg mL^{-1} of polymer and cast in the glove box to form a 100 nm thick layer. The substrates were then kept in a vacuum of $\approx 10^{-2}$ mbar for 2 h. Subsequently, another D-PEDOT:PSS layer was deposited.

PMDPP3T:PC_{60}BM Single Junction Cells: Sol–gel ZnO was processed on the clean ITO substrate. PMDPP3T was blended with $PC_{60}BM$ (1:3 weight ratio) and dissolved in a solution of chloroform, containing 7 vol% *o*-dichlorobenzene. The concentration of the polymer was 3 mg mL^{-1}. The solution of PMDPP3T:PC_{60}BM was spin coated in ambient air to obtain a layer 170 nm in thickness. After this, a layer of D-PEDOT:PSS was spin coated on top.

PDPPSDTPS:PC_{60}BM Single Junction Cells: D-PEDOT:PSS was processed directly on clean ITO substrates, followed by a layer of ZnO nanoparticles. PDPPSDTPS was blended with $PC_{60}BM$ (1:2 weight ratio) and together dissolved in chloroform, containing 5 vol% *o*-dichlorobenzene. The concentration of the polymer was 4 mg mL^{-1}. The active layer was spin coated in the glove box, with a thickness of 160 nm.

Quadruple Junction Solar Cells: Sol–gel ZnO was spin coated on clean ITO substrates. A layer of 110 nm of PDCBT:PC_{60}BM was processed on top in a glove box and annealed at 100 °C for 5 min. Subsequently, the first layer of D-PEDOT:PSS was spin coated and annealed in a glove box, at 105 °C for 10 min. To finish the first ICL, ZnO nanoparticles were spin coated on D-PEDOT:PSS, followed by 100 nm of PTB7-Th:PC_{70}BM. After this step, the samples were dried in a vacuum of $\approx 10^{-2}$ mbar for 2 h. For the second ICL, D-PEDOT:PSS was spin coated again. Then the ZnO nanoparticles layer was deposited, followed by 170 nm of PMDPP3T:PC_{60}BM. The third ICL was again fabricated with a D-PEDOT:PSS layer, followed by the ZnO nanoparticles. The last active layer was deposited in the glove box with a thickness of 160 nm. The cell was completed by the thermal evaporation of MoO_x (10 nm) and Ag (100 nm) at $\approx 6 \times 10^{-7}$ mbar.

Characterization: Both the measurements of the *J–V* curve and the EQE were performed under nitrogen atmosphere. The substrates were treated under a UV lamp for 8 min before measuring, in order to photodope the ZnO and MoO_X layers. Subsequently, the *J–V* characteristics were measured with a Keithley 2400 source meter from −2 to +2 V (single junction cells) and from −2 to +3 V (quadruple junction cells). Four hundred and one points per scan were acquired, each with 20 ms integration time. The lamp used for this measurement was a tungsten-halogen lamp, which was filtered with a UV filter and a daylight filter (Hoya LB120), calibrated to match the current integrated from the EQE spectrum of each single junction cell, as shown in the text. The measurements were performed through an illumination mask with aperture sizes of 6.76 and 12.96 mm^2, corresponding to the 9 and 16 mm^2 nominal device areas, respectively. This defined the active area of the devices.

The EQE measurement was performed in a home-made setup, consisting of a tungsten-halogen lamp, a chopper, a monochromator (Oriel, Cornerstone 130), a pre-amplifier (Stanford Research Systems SR570), and a lock-in amplifier (Stanford Research Systems SR830 DSP). The substrates were kept in a N_2-filled box with a quartz window during the duration of the measurement. The device of interest on each substrate was aligned through a circular aperture with 2 mm of diameter, defining the active area. The signal response to the modulated light was transformed into an EQE value by comparison with the measurement on a calibrated silicon reference solar cell. The average standard deviation in measuring the wavelength-dependent EQE measurement

in this setup is less than 0.005 in electrons/photons for wavelengths in the range of 350–1050 nm. The 530, 730, and 940 nm bias lights were high-power LEDs obtained from Thorlabs. The additional voltage bias was applied directly from the pre-amplifier. The V_{OC} of the representative single junction cells under simulated AM1.5G spectrum was measured and those values were used to estimate the voltage bias needed for each light bias condition. In particular, the voltage correction was the sum of the V_{OC}s of the optically biased subcells for each case. Since the aperture for the measurement of the EQE was smaller (3.14 mm^2) than the apertures used for the measurement of the *J–V* characteristic (6.76 and 12.96 mm^2), another mask with a 3.14 mm^2 aperture to measure again the representative single junction cells was used. The measurement returned V_{OC}s of 0.80, 0.75, 0.58, and 0.27 V for the PDCBT, PTB7-Th, PMDPP3T, and the PDPPSDTPS single cells.

Optical Modeling: Optical modeling based on the TM method was performed using Setfos 3.2 (Fluxim). The wavelength-dependent *n* and *k* values of each active layer were determined by transmission and reflection measurements using an integrating sphere attachment on a Perkin-Elmer Lambda 1050 spectrophotometer. More details about the procedure are provided in the Supporting Information. The optimization based on IQE correction of the modeled current densities and the construction of the *J–V* characteristics were performed according to a procedure previously reported and extended for quadruple junction cells (please refer to the Supporting Information for more details).[28] In order to fine tune the prediction with a more accurate estimate of the J_{SC} generated in each subcell, the IQE was determined as a function of the wavelength (λ). To calculate IQE(λ), the EQEs of the representative single junction cells were divided (Tables S1–S4, Supporting Information) by the corresponding fractions of absorbed photons ($f_A(\lambda)$) of the active layers, estimated by means of optical modeling. Again, using the optical modeling, $f_A(\lambda)$ for each active layer in the quadruple junction cell was calculated and these spectra were multiplied by the corresponding IQE(λ), obtaining an estimated EQE value. The calculation of the J_{SC} value was then followed by integration with the AM1.5G reference spectrum. The same tools were used to predict the current generation of each subcell in the quadruple junction cell under the different light bias conditions. This was done by measuring the power density of the light sources at a different driving current with the calibrated silicon reference cell of the EQE setup and scaling the power profile of each LED (provided by the manufacturer) by those values. The latter spectra were used as input for the TM calculation.

Supporting Information

Supporting Information is available from the Wiley Online Library or from the author.

Acknowledgements

The authors thank Dr. Harm van Eersel for developing scripts to calculate the optoelectrical parameters and Robin Willems for helping in the synthesis of the ZnO nanoparticles. This project received funding from the European Community's Seventh Framework Programme (FP7/2007–2013) under the Grant Agreement No. 607585 project OSNIRO. The research leading to these results has also received funding from the European Research Council under the European Union's Seventh Framework Programme (FP/2007–2013) / ERC Grant Agreement No. 339031. The research also received funding from the Ministry of Education, Culture and Science (Gravity program 024.001.035).

Conflict of Interest

The authors declare no conflict of interest.

Keywords

conjugated polymers, fullerenes, polymer solar cells, quadruple junction

Received: June 17, 2018
Revised: July 13, 2018
Published online: August 23, 2018

[1] M. Kaltenbrunner, M. S. White, E. D. Glowacki, T. Sekitani, T. Someya, N. S. Sariciftci, S. Bauer, *Nat. Commun.* **2012**, *3*, 1772.
[2] R. Ma, J. Feng, D. Yin, H.-B. Sun, *Org. Electron.* **2017**, *43*, 77.
[3] Y. Li, G. Xu, C. Cui, Y. Li, *Adv. Energy Mater.* **2018**, *8*, 1701791.
[4] K.-S. Chen, J.-F. Salinas, H.-L. Yip, L. Huo, J. Hou, A. K.-Y. Jen, *Energy Environ. Sci.* **2012**, *5*, 9551.
[5] C.-C. Chen, L. Dou, J. Gao, W. H. Chang, G. Li, Y. Yang, *Energy Environ. Sci.* **2013**, *6*, 2714.
[6] G. Xu, L. Shen, C. Cui, S. Wen, R. Xue, W. Chen, H. Chen, J. Zhang, H. Li, Y. Li, Y. Li, *Adv. Funct. Mater.* **2017**, *27*, 1605908.
[7] G. Li, R. Zhu, Y. Yang, *Nat. Photonics* **2012**, *6*, 153.
[8] R. Søndergaard, M. Hösel, D. Angmo, T. T. Larsen-Olsen, F. Krebs, *Mater. Today* **2012**, *15*, 36.
[9] A. Reale, L. La Notte, L. Salamandra, G. Polino, G. Susanna, T. M. Brown, F. Brunetti, A. Di Carlo, *Energy Technol.* **2015**, *3*, 385.
[10] W. Zhao, S. Li, H. Yao, S. Zhang, Y. Zhang, B. Yang, J. Hou, *J. Am. Chem. Soc.* **2017**, *139*, 7148.
[11] S. Zhang, Y. Qin, J. Zhu, J. Hou, *Adv. Mater.* **2018**, *30*, 1800868.
[12] A. Brown, M. Green, *Prog. Photovolt.: Res. Appl.* **2002**, *10*, 299.
[13] P. T. Chiu, D. C. Law, R. L. Woo, S. B. Singer, D. Bhusari, W. D. Hong, A. Zakaria, J. Boisvert, S. Mesropian, R. R. King, N. H. Karam, Proc. 2014 IEEE 40th Photovoltaic Specialist Conf. (PVSC), Institute of Electrical and Electronics Engineers Inc., Denver, CO, USA **2014**, p. 0011.
[14] B. Liu, L. Bai, T. Li, C. Wei, B. Li, Q. Huang, D. Zhang, G. Wang, Y. Zhao, X. Zhang, *Energy Environ. Sci.* **2017**, *10*, 1134.
[15] A. Furlan, R. A. J. Janssen, in *Polymer Photovoltaics: Materials, Physics, and Device Engineering* (Eds: F. Huang, H.-L. Yip, Y. Cao), Royal Society of Chemistry, London, UK **2015**, Ch. 11, pp. 310–351.
[16] G. Li, W. H. Chang, Y. Yang, *Nat. Rev. Mater.* **2017**, *2*, 1.
[17] X. Che, Y. Li, Y. Qu, S. R. Forrest, *Nat. Energy* **2018**, *3*, 422.
[18] N. Li, D. Baran, K. Forberich, M. Turbiez, T. Ameri, F. C. Krebs, C. J. Brabec, *Adv. Energy Mater.* **2013**, *3*, 1597.
[19] J. Gilot, R. A. J. Janssen, in *Organic Solar Cells: Fundamentals, Devices, and Upscaling* (Eds: B. P. Rand, H. Richter), Pan Stanford Publishing Pte. Ltd., Singapore **2014**, Ch. 6, pp. 277–313.
[20] D. Di Carlo Rasi, K. H. Hendriks, M. M. Wienk, R. A. J. Janssen, *Adv. Energy Mater.* **2017**, *7*, 1701664.
[21] M. Zhang, X. Guo, W. Ma, H. Ade, J. Hou, *Adv. Mater.* **2014**, *26*, 5880.
[22] S. H. Liao, H. J. Jhuo, Y. S. Cheng, S. A. Chen, *Adv. Mater.* **2013**, *25*, 4766.
[23] W. Li, A. Furlan, K. H. Hendriks, M. M. Wienk, R. A. J. Janssen, *J. Am. Chem. Soc.* **2013**, *135*, 5529.
[24] K. H. Hendriks, W. Li, M. M. Wienk, R. A. J. Janssen, *J. Am. Chem. Soc.* **2014**, *136*, 12130.
[25] D. Di Carlo Rasi, K. H. Hendriks, G. H. L. Heintges, G. Simone, G. H. Gelinck, V. S. Gevaerts, R. Andriessen, G. Pirotte, W. Maes, W. Li, M. M. Wienk, R. A. J. Janssen, *Sol. RRL* **2018**, *2*, 1800018.
[26] J. Gilot, M. M. Wienk, R. A. J. Janssen, *Adv. Funct. Mater.* **2010**, *20*, 3904.
[27] D. Bahro, M. Koppitz, A. Mertens, K. Glaser, J. Mescher, A. Colsmann, *Adv. Energy Mater.* **2015**, *5*, 1501019.
[28] J. Gilot, M. M. Wienk, R. A. J. Janssen, *Adv. Mater.* **2010**, *22*, E67.